

Approximate buckling strength analysis of arbitrarily stiffened, stepped plates

Lars Brubak*, Jostein Helleland

Mechanics Division, Department of Mathematics, University of Oslo, NO-0316 Oslo, Norway

Received 23 May 2006; received in revised form 28 November 2006; accepted 4 December 2006

Available online 11 January 2007

Abstract

A computationally efficient method for the elastic buckling and buckling strength analysis of in-plane biaxial and shear loaded stiffened plates with varying, stepwise constant thickness is presented. The main focus is on biaxial loading cases. The stiffeners may be sniped or end-loaded (continuous), and their orientations may be arbitrary. Both global and local plate buckling modes are captured. The method is semi-analytical and makes use of simplified displacement computations that involve the elastic buckling load (eigenvalue), determined using a Rayleigh–Ritz approach, and finally stress computations using large deflection theory in combination with strength assessment using von Mises' yield criterion as applied to membrane stresses. The displacements are represented by trigonometric functions, defined over the entire plate. The method is implemented into a Fortran computer program, and numerical results, obtained by the method for a variety of plate and stiffener geometries, are compared with corresponding fully nonlinear finite element analysis results. An extension to strength analysis that also includes lateral loading is discussed.

© 2006 Elsevier Ltd. All rights reserved.

Keywords: Stiffened plates; Stepped plate; Arbitrary stiffener orientations; Buckling strength; Elastic buckling load; Semi-analytical method

1. Introduction

In many branches of engineering, stiffened plates are used as one of the main structural components in order to improve the strength/weight ratios and reduce costs of structures. For analysis of large structures, computationally efficient analysis tools are useful for obtaining results within a reasonable time limit. Also, such tools may be a necessity for the design of structures with complex geometry and complex stiffener arrangements, for which explicit strength formulae [1–3] may not be applicable. Nonlinear finite element method analyses could be used in such cases. However, such analyses are often time consuming to prepare, run and post-process, and other approaches may be better suited in more practically oriented design contexts.

Computationally efficient analysis tools using semi-analytical methods for buckling and ultimate strength predictions are becoming more common. A rather advanced

nonlinear buckling model was developed by Byklum et al. [4, 5], based on previous work by Steen [6,7]. These studies deal mainly with unstiffened and regularly stiffened plates. A related model, presented in Brubak, Helleland and Steen [8], deals with buckling strength analysis of constant thickness plates provided with sniped stiffeners with irregular orientations. These models have been adopted by the ship classification and engineering services company Det Norske Veritas (DNV), and implemented into a computerised software code entitled PULS [9]. The semi-analytical models above are based on the Rayleigh–Ritz method. A more detailed review of semi-analytical methods that make use of this method, as well as of the Galerkin method (Paik and Lee [10], etc.), is given in Brubak et al. [8].

The studies mentioned above deal with plates of constant thickness. Sometimes, it is advantageous to vary the plate thickness locally to increase the buckling strength and obtain more cost efficient structures. Several approaches have been formulated for such plates. For example, Azhari, Shahidi and Saadatpour [11] presented a semi-analytical method for analysing the post-buckling behaviour of initially perfect,

* Corresponding author. Tel.: +47 22855990.

E-mail address: lbrubak@math.uio.no (L. Brubak).

Notation

a_{ij}	Displacement amplitudes
b	Plate width (in y -direction)
b_e	Effective plate width
b_s	Width of plate strip number s
D_s	$= Et_s^3/12(1 - \nu^2)$ Plate strip bending stiffness
E	Young's modulus
f_Y	Yield strength
I_e	Effective moment of inertia of stiffener
L	Plate length (in x -direction)
P_{xy}	External shear load
\bar{S}_x, \bar{S}_y	External stresses (positive in compression)
t_s	Thickness of plate strip number s
w	Out-of-plane displacements (z -direction)
w_0	Model imperfection
$w_{,g}$	$= \partial w / \partial g$
$w_{,gh}$	$= \partial^2 w / \partial g \partial h$
ν	Poisson's ratio
σ_x, σ_y	In-plane stresses (positive in tension)
τ_{xy}	In-plane shear stress

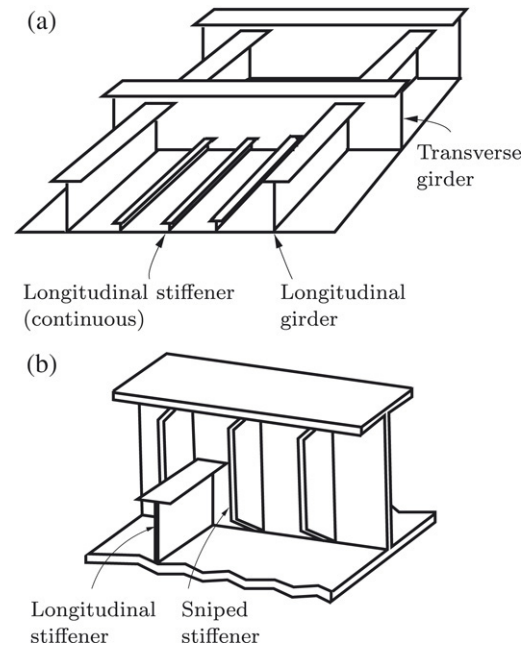


Fig. 1. Examples of stiffened plates: (a) Stiffened plate enclosed by longitudinal and transverse girders, and (b) girder stiffened by sniped stiffeners.

unstiffened stepped plates (i.e., with varying, stepwise constant thickness). Xiang and Wei [12] developed a method for the linear elastic buckling and vibration analysis of such plates. These two papers summarise some earlier works on stepped plates. Most of these works deal mainly with unstiffened plates and not with the buckling strength of imperfect plates (onset of yielding, capacity etc.) as such.

The main objective of the present paper is to present and document the applicability of a semi-analytical model for the local and global buckling strength analysis of uni-directionally stepped plates. It represents an extension of an earlier work [8] on constant thickness plates with sniped stiffeners. The present study also includes extensions to end-loaded (continuous) stiffeners and torsional stiffness considerations, but does not include the local failure modes of the stiffeners. The plates may have regular or arbitrarily oriented stiffeners, and may have various restraints at the plate edges and in the interior of the plate.

The scope of the present paper is limited to the topic of buckling and buckling strength. However, the presented model can readily be extended to strength computations of plates that also include lateral loading. The additions required to accommodate such extensions are also presented.

2. Stiffened plate modelling

Two stiffened plate examples are shown in Fig. 1. The stiffeners of a plate enclosed by the strong longitudinal and transverse girders in Fig. 1(a), are typically continuous and subject to axial loading at their ends (at the plate boundary). Unlike these, the sniped (“discontinuous”) stiffeners illustrated on the girder web in Fig. 1(b), will not be axially loaded at their ends. Normally, this will also be the case for non-regular

stiffeners, such as, for instance, in the stern and bow of a ship hull.

The plate considered can be defined with reference to Fig. 2. The plate may consist of an arbitrary number of uni-directional plate strips of different thickness (3 shown in the figure). It may be provided with one or several stiffeners with arbitrary orientations. The stiffeners may be sniped at the ends or end-loaded (continuous). They may have different cross-section profiles, and may be eccentric, as in Fig. 2(b), or symmetric about the middle plane of the plate.

The stiffeners are modelled as simple beams with flexural stiffness only against out-of-plane bending. This implies that possible local buckling of stiffeners, including torsional instability, cannot be predicted. This may not represent a serious limitation in practical cases, as design rules generally impose constructional design provisions that prevent any local buckling of the stiffeners. For instance, compression parts, such as T-stiffeners, subjected to a constant stress are capable according to Eurocode 3 [13] of developing full plastic moment resistance before the onset of local buckling, provided

$$c_w/t_w \leq 38\sqrt{235/f_Y}; \quad c_f/t_f \leq 10\sqrt{235/f_Y}. \quad (1)$$

Here, f_Y is the yield strength (in MPa), c_w is the free or unsupported web height (e.g., the clear distance between the welds at the ends of the web), and c_f is the unsupported flange outstand. More slender stiffeners are allowed for situations with no yielding in the extreme fibres, or for stiffeners subjected to both membrane and bending stress. Similar constructional design rules can be found in DNV's recommended practice [3].

Also, stiffeners are usually proportioned, for instance using the present model, so as to provide sufficient strength to prevent a global plate buckling mode. Without the additional axial

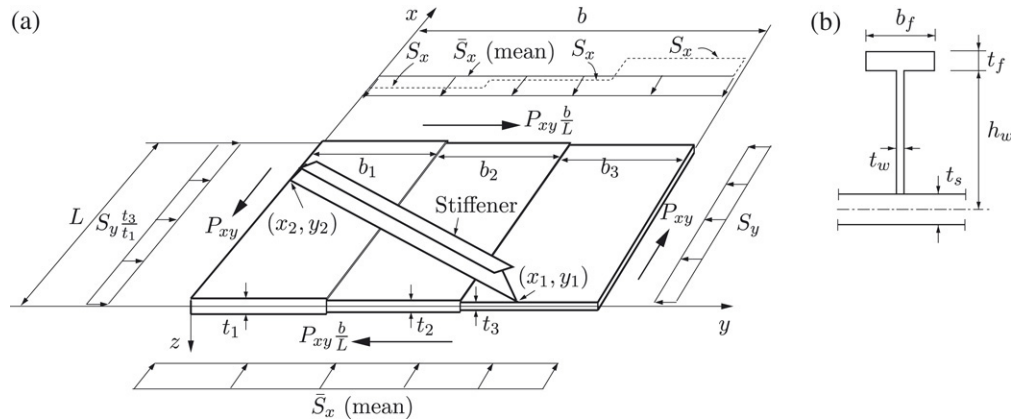


Fig. 2. Simply supported plate with varying, stepwise constant plate thicknesses, subjected to external in-plane compression or tension \bar{S}_x and S_y in the x - and y -direction, respectively, and a shear stress resultant P_{xy} .

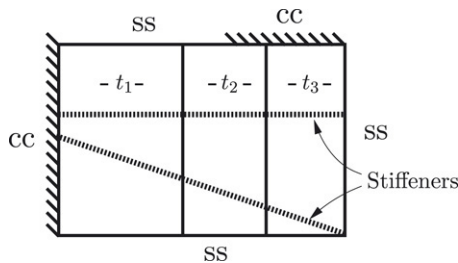


Fig. 3. Stepped plate example with partly simple (ss) and partly clamped supports (cc), and irregular stiffener arrangement.

stress from global bending, local buckling of stiffeners is even less likely. Thus, the simplified stiffener model seems like a reasonable one.

The torsional stiffness of the stiffeners may be included, but their axial stiffness is neglected. The latter implies that the stiffeners' effect on the internal membrane stress distribution in the plate is neglected. This is considered an acceptable simplification.

The usual assumptions that the plate edges remain straight (due to the neighbouring plates) while in-plane movements are allowed, are adopted. Otherwise, all four plate edges are supported in the out-of-plane direction. An edge, or a part of an edge, may rotationally be simply supported, or partly or fully clamped, as illustrated in Fig. 3. Rotational and out-of-plane restraints, modelled by strong translational and rotational springs, can also be added along specified lines with arbitrary orientations in the interior of the plate.

The displacement field is defined over the entire plate. It was initially questioned whether this was adequate for stepped plates. Preliminary eigenvalue and buckling strength results obtained indicated that it is. The alternative of specifying one displacement field for each plate strip and imposing continuity requirements along the boundaries between the plate strips, is considerably more complicated and was not considered.

Hooke's material law for plane stress for an elastic, isotropic material is adopted, and further, Kirchhoff's deformation assumption (a straight line normal to the middle plane prior to loading, remains straight and normal to the plane after

deformation). These are the usual thin plate assumptions [14]. The first implies that only in-plane stresses (σ_x , σ_y , τ_{xy}) and in-plane strains (ϵ_x , ϵ_y , γ_{xy}) are present. The second implies that the strains, consisting of membrane strains (constant over the plate thickness) and bending strains, vary linearly across the plate thickness.

The plate, Fig. 2, may be subjected to in-plane compressive or tensile loading, and to in-plane shear loading. The former are defined in the figure in terms of \bar{S}_x and S_y , and the latter in terms of the edge resultant P_{xy} .

Two approaches are considered for computing initial plate stresses due to the shear loading: (1) a simplified approach (Section 4) suitable for plates with limited, but practical, thickness variations, and (2) a more advanced approach (Section 13) that has not yet been implemented.

3. Major computational steps

The computations are carried out in two major steps:

1. In the first step, labelled the elastic buckling stress limit (ESL) state, the elastic buckling load (first eigenvalue) and the corresponding buckling mode of the stiffened plate are calculated.
2. In the second step, labelled the buckling strength limit (BSL) state, a buckling strength (capacity) assessment is made for the plate, with a specified out-of-plane imperfection. This step involves displacement computations using an approximate displacement magnifier (based on small deflection theory) that is a function of the applied load and the elastic buckling load (ESL); computation of stresses according to large deflection theory; and, finally, strength assessment using the von Mises yield criterion as applied to the membrane stresses.

The essential parts of the model are described below. Additional details are given in Brubak [15].

4. Initial, reference membrane stresses

In order to determine the initial, reference biaxial membrane stresses in the various plate strips, a linear static analysis is

performed for a perfect plate with a chosen reference loading (\bar{S}_{x0} and S_{y0} , positive in compression). For illustration, the stepped plate shown in Fig. 4(a) can be considered. It consists of three plate strips and has four in-plane degrees of freedom, d_1 to d_4 . Stiffeners are not included (their axial stiffness is neglected). The resulting axial plate stiffness relationship can be given in matrix form by

$$\mathbf{K}_0 \mathbf{d} = \mathbf{P}_0 \quad (2)$$

where

$$\mathbf{K}_0 = E^* \begin{bmatrix} \sum_{i=1}^2 \frac{t_i L}{b_i} & -\frac{t_2 L}{b_2} & 0 & \nu(t_1 - t_2) \\ -\frac{t_2 L}{b_2} & \sum_{i=2}^3 \frac{t_i L}{b_i} & -\frac{t_3 L}{b_3} & \nu(t_2 - t_3) \\ 0 & -\frac{t_3 L}{b_3} & \frac{t_3 L}{b_3} & \nu t_3 \\ \nu(t_1 - t_2) & \nu(t_2 - t_3) & \nu t_3 & \sum_{i=1}^3 \frac{t_i b_i}{L} \end{bmatrix} \quad (3)$$

$$\mathbf{d} = [d_1, d_2, d_3, d_4]^T \quad (4)$$

$$\mathbf{P}_0 = [0, 0, -P_{y0}, -P_{x0}]^T. \quad (5)$$

Here, $E^* = E/(1 - \nu^2)$, E and ν are Young's modulus and Poisson's ratio, respectively, $P_{x0} = \bar{S}_{x0}(b_1 t_1 + b_2 t_2 + b_3 t_3)$ and $P_{y0} = S_{y0} L t_3$ are the resultant, reference forces acting on the plate edges. Once Eq. (2) is solved, the initial reference strains can be computed from

$$\epsilon_{x0} = \frac{d_4}{L} \quad \text{and} \quad \epsilon_{y0} = \begin{cases} d_1/b_1 \\ (d_2 - d_1)/b_2 \\ (d_3 - d_2)/b_3 \end{cases} \quad (6)$$

for plate strips 1, 2 and 3, respectively. Inserted into Hooke's law, these strains give initial, reference membrane stresses σ_{x0}^m and σ_{y0}^m that are constant within each of the plate strips. These strains and stresses are defined as positive when tensile (i.e., the opposite of the externally applied stress definition). A consequence of the straight edge assumption is that the resultant of the mean external stress \bar{S}_x , in the x -direction, will initially be distributed as illustrated in Fig. 2 by the varying, stepwise constant stress S_x .

The initial stress distribution due to the shear loading is considerably more complicated. Due to the straight edge assumption, the varying plate thickness causes the development of both shear stresses and additional axial stresses. The shear stress varies both within a specific plate strip and between strips. In order to properly account for these shear and axial stresses, it is necessary to carry out an analysis based on a multi-degree-of-freedom, in-plane displacement field, as discussed later (Section 13).

However, for plates with limited thickness variations of about 10%–20% between adjacent plate strips, simplifications can be justified. Finite element analyses of stress distributions have been carried out for a number of such plates with shear loading, Fig. 4(b). The results show (1) that axial stresses are

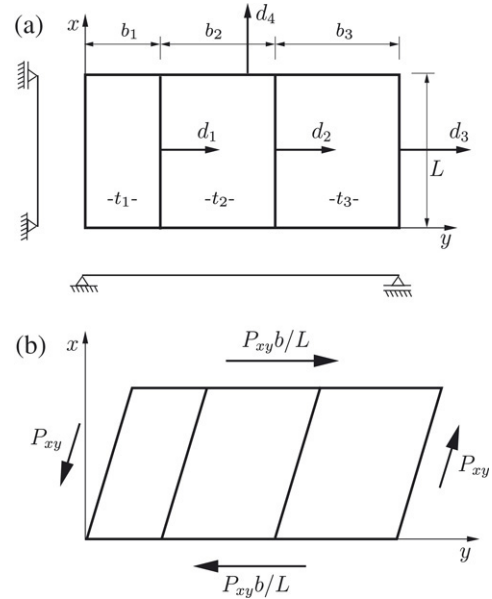


Fig. 4. (a) In-plane degrees of freedom due to a biaxial load case and (b) in-plane deformation shape due to a shear loading for a stepped plate example with three plate strips.

rather small and can be neglected, and (2) that shear stresses are rather constant over the total plate and are approximately equal to

$$\tau_{xy0}^m = \frac{P_{xy0} \frac{b}{L}}{b_1 t_1 + b_2 t_2 + b_3 t_3} \quad (7)$$

where P_{xy0} is the reference value of P_{xy} and τ_{xy0} is the reference shear stress in the plate. The premise for these results is that the edges, forming a parallelogram, are straight and parallel to their opposite edges, and further, that the elongation of any parts of the edges is zero (i.e., there is zero axial strain in the edge direction at the edges). This simplified, initial shear stress is adopted here.

5. Elastic buckling stress limit (ESL)

In the first step of the analysis, the elastic buckling load (first eigenvalue) of a perfect, stiffened plate is computed using the Rayleigh–Ritz method. For completeness and for the convenience of the reader, the major elements are summarised below. The assumed out-of-plane displacement field, which satisfies the boundary conditions of a simply supported plate, is given by

$$w(x, y) = \sum_{i=1}^M \sum_{j=1}^N a_{ij} \sin\left(\frac{\pi i x}{L}\right) \sin\left(\frac{\pi j y}{b}\right) \quad (8)$$

where a_{ij} are amplitudes to be determined, L is the plate length, b is the total plate width, $0 \leq x \leq L$ and $0 \leq y \leq b$.

Although each component in a series of sine functions represents a simply supported condition, added together they are, in combination with rotational springs along the supports, nearly able also to describe fully or partially restrained conditions [4,15]. Therefore, rather than specifying different fields, such as for instance a series of cosine functions for a clamped plate, the sine curve assumption is used for various

boundary conditions. To achieve the same accuracy, a higher number of degrees of freedom (number of terms) will normally be required with a sine field than with a field that satisfies the kinematic boundary conditions more appropriately.

Equilibrium of the loaded plate requires that its total potential energy, $\Pi = U + T$, has a stationary value, i.e., $\delta\Pi = \delta(U + T) = 0$. Here, U is the strain energy and T is the potential energy of the external loads. This requirement leads to the eigenvalue problem

$$(\mathbf{K}^M + \Lambda^e \mathbf{K}^G) \mathbf{a}^e = \mathbf{0} \quad (9)$$

where \mathbf{K}^M is the material stiffness matrix (due to U), \mathbf{K}^G the geometrical stiffness matrix (due to T for the initial, reference loading), Λ^e are the eigenvalues (load factors at buckling), and \mathbf{a}^e are the eigenvectors containing all the displacement amplitudes a_{ij} that together define the buckling mode for a specific eigenvalue. The energy contributions used in the derivation of the eigenvalue problem are given below. The strain energy from membrane stresses is not included, as it does not affect computed eigenvalues.

The elastic strain energy from bending of the entire plate, U_{plate}^b , is obtained by adding up the contributions U_s^b from each plate strip s . With N_s number of plate strips, the total bending strain energy becomes

$$U_{\text{plate}}^b = \sum_{s=1}^{N_s} U_s^b \quad (10)$$

where

$$U_s^b = \int_0^L \int_{y_{s1}}^{y_{s2}} \frac{D_s}{2} \left((w_{,xx} + w_{,yy})^2 - 2(1-\nu)(w_{,xx}w_{,yy} - w_{,xy}^2) \right) dx dy \quad (11)$$

is the contribution from plate strip number s , located between $y = y_{s1}$ and $y = y_{s2}$, with thickness t_s and flexural plate stiffness $D_s = Et_s^3/12(1-\nu^2)$, and where the conventional ‘‘comma’’ notation $w_{,xy}$ for $\partial^2 w/\partial x \partial y$, etc., is adopted. By substituting the assumed displacement field, an analytical solution of this integral may be derived and written in the form:

$$U_s^b = \sum_{i=1}^M \sum_{j=1}^N \sum_{l=1}^N a_{ij} a_{il} \frac{D_s L}{4} \left[\left(\left(\frac{\pi i}{L} \right)^2 + \left(\frac{\pi j}{b} \right)^2 \right) \times \left(\left(\frac{\pi i}{L} \right)^2 + \left(\frac{\pi l}{b} \right)^2 \right) \times H_1(j, l) - 2(1-\nu) \left(\left(\frac{\pi i}{L} \right)^2 \left(\frac{\pi l}{b} \right)^2 H_1(j, l) - \left(\frac{\pi i}{L} \right)^2 \frac{\pi j}{b} \frac{\pi l}{b} H_2(j, l) \right) \right] \quad (12)$$

where $H_1(j, l)$ and $H_2(j, l)$ are given in Appendix A. Note that b and L are the total plate dimensions. For a constant thickness plate, i.e. a plate with only one plate strip, $H_1(j, l) = H_2(j, l) = 0$, if $j \neq l$, and $H_1(j, j) = H_2(j, j) = b/2$. Thus,

Eq. (12) breaks down into the more well known double sum for that case.

Similarly, the potential energy of the external plate loads can be given by

$$T = \sum_{s=1}^{N_s} T_s \quad (13)$$

where

$$T_s = \Lambda \int_0^L \int_{y_{s1}}^{y_{s2}} \frac{t_s}{2} (\sigma_{x0} w_{,x}^2 + \sigma_{y0} w_{,y}^2 + 2\tau_{xy0} w_{,x} w_{,y}) dy dx \quad (14)$$

in the case of proportional loading. Here, Λ is the load factor. By the substitution of the initial internal stresses, the analytical solution of this integral can be written as

$$T_s = \Lambda \sum_{i=1}^M \sum_{j=1}^N \sum_{l=1}^N a_{ij} a_{il} \left(\frac{\sigma_{x0}^m t_s (i\pi)^2}{4L} H_1(j, l) + \frac{\sigma_{y0}^m t_s L j l \pi^2}{4b^2} H_2(j, l) \right) + \Lambda \sum_{i=1}^M \sum_{j=1}^N \sum_{k=1}^M \sum_{l=1}^N a_{ij} a_{kl} \frac{\tau_{xy0}^m t_s \pi^2 i l}{Lb} H_3(j, l) H_4(i, k) \quad (15)$$

where $H_3(j, l)$ and $H_4(i, k)$ are given in Appendix A. The effect of a constant uniaxial or biaxial pre-stress of the plate can readily be included above, by adding another term that is not increased by the load factor Λ . In the same manner as for the strain energy of the plate, the first part (triple series) of Eq. (15) breaks down into the more well known double sum for constant thickness plates.

The curvature of a stiffener is equal to the curvature of the plate along the stiffener. Then, for an arbitrarily oriented stiffener with length L_s , end coordinates (x_1, y_1) and (x_2, y_2) , and cross-section area A_s , the bending strain energy due to the stiffener can be given by

$$U_{\text{stiff}}^b = \frac{EI_e}{2} \int_{L_s} w_{,ss}^2 dL_s = \frac{EI_e}{2L_s^4} \int_{L_s} (L_x^2 w_{,xx} + 2L_x L_y w_{,xy} + L_y^2 w_{,yy})^2 dL_s \quad (16)$$

where I_e is an effective moment of inertia about the axis of bending, $w_{,ss}$ the curvature in the stiffener direction, $L_x = (x_2 - x_1)$ and $L_y = (y_2 - y_1)$. In the case of an eccentric stiffener, the stiffener will ‘‘lift’’ the axis of bending above the middle plane. I_e can be given by

$$I_e = \int_{A_s} (z - z_c)^2 dA_s + b_e t z_c^2 \quad (17)$$

where z_c is the distance from the plate middle plane to the centroidal axis (through the centre of area) of a section consisting of the stiffener and an effective plate area of width b_e . For a stepped plate, t may conservatively be taken as the thickness of the thinnest of the plate strips. The bending of the

plate about its own axis (middle plane) is included in the plate strain energy. The strain energy integral above may be solved analytically or by numerical integration. The latter is chosen here.

For a symmetric stiffener, $z_c = 0$ is the correct solution, as bending in this case will be about the middle plane. For an eccentric stiffener, Eq. (17) is an approximation, whose accuracy will depend on the assumed value of b_e . It is found that $z_c = 0$ is an acceptable value for eccentric stiffeners in many practical cases as well. In practical design work, a z_c -value calculated with a b_e of about $b_e = 20t$ has been suggested [8, 15].

The torsional stiffness of the stiffeners may be accounted for by including the energy contribution (St. Venant torsion) given by

$$\begin{aligned} U_{\text{stiff}}^T &= \frac{GJ}{2} \int_{L_s} w_{,ns}^2 dL_s \\ &= \frac{GJ}{2L_s^4} \int_{L_s} \left(L_x L_y (w_{,yy} - w_{,xx}) + (L_x^2 - L_y^2) w_{,xy} \right)^2 dL_s \end{aligned} \quad (18)$$

where J is the torsion constant, $w_{,ns}$ is the partial double derivative of w with respect to the directions normal to and along the stiffener, and $G = E/2(1 + \nu)$.

For end loaded (continuous) stiffeners, it is necessary to include the potential energy due to external loads on the stiffener ends. For the arbitrarily oriented stiffener considered above, it can be shown that its effect due to plate shortening can be expressed by

$$\begin{aligned} T_{\text{stiff}} &= -\Lambda \frac{P_{s0}}{2} \int_{L_s} w_{,s}^2 dL_s \\ &= -\Lambda \frac{P_{s0}}{2L_s^2} \int_{L_s} (L_x w_{,x} + L_y w_{,y})^2 dL_s \end{aligned} \quad (19)$$

where P_{s0} is the initial, resultant reference load on the stiffener. It acts in the stiffener direction, and it is defined to be positive in compression. The translation of this load due to the rotation of the stiffener end is not included, as it does not affect the computed eigenvalues.

If plate edges, or portions of edges, are partly or fully clamped (modelled by rotational springs), additional strain energy contributions have to be added. Similarly, contributions have to be added for any rotational or translational restraints in the interior of the plate. For additional details, see Brubak et al. [8,15].

6. Buckling strength limit (BSL)

6.1. Load incrementation and strength criterion

The present model aims at predicting an approximate buckling strength limit (BSL) of a stiffened plate with an initial displacement imperfection (w_0). Additional displacements (w) at a given load stage are estimated using the approximate displacement magnifier

$$w = \frac{\Lambda}{\Lambda_{cr}^e - \Lambda} w_0 \quad (20)$$

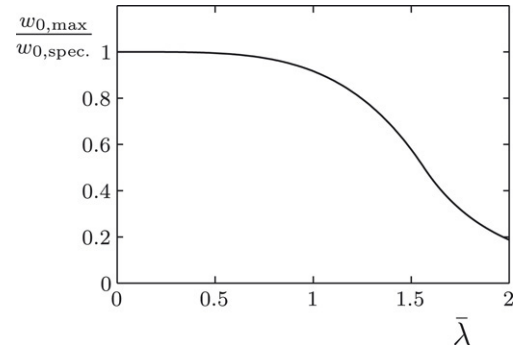


Fig. 5. Adopted maximum imperfection amplitude versus reduced slenderness.

where Λ_{cr}^e is the load factor of the first eigenvalue, and Λ is the load factor at a given stage of the loading ($\Lambda \bar{S}_{x0}$, ΛS_{y0} , ΛP_{xy0}).

This, and similar magnifiers based on linearised elastic second order theory (small deflection theory), are commonly used for approximate analyses of both columns and plates [14]. The load factor, and the resulting displacements and stresses, redistributed due to the out-of-plane displacements, are increased until the adopted strength criterion (below) is satisfied.

The use of Eq. (20) implies that the buckling strength estimate will never exceed the elastic buckling load limit. In order to capture the load carrying capability of slender (thin) plates beyond this limit, often denoted as the post-critical (or reserve) strength, displacements must be computed using large displacement theory. However, in practical design, it may be desirable not to utilise this reserve strength, in order to limit formation of any significant plastic (permanent) deformations of slender plates. It is in such contexts that the present model represents a sound alternative.

A buckling strength criterion, proposed and discussed previously [8], is adopted for the presented model. According to this criterion, the buckling strength is obtained at the first yield according to the von Mises' yield criterion [14], applied to membrane stresses:

$$\sigma_e^m = \sqrt{(\sigma_x^m)^2 + (\sigma_y^m)^2 - \sigma_x^m \sigma_y^m + 3(\tau_{xy}^m)^2} = f_Y. \quad (21)$$

This membrane stress criterion allows, in an approximate manner, for some additional strength due to the redistribution of stresses after yielding in the outer plate fibres.

The critical stress points are typically located in the plate along the edges, along the stiffeners, or at the boundary between two neighbouring plate strips. The latter is typical for a plate strip subjected mainly to a stress in the x -direction and that is located between two considerably thicker plate strips, that prevent out-of-plane displacements along its boundaries.

6.2. Imperfection shape and amplitude

The imperfection shape can be taken according to any specified shape. Here, w_0 is taken to be equal to the first buckling mode (eigenmode) from the ESL analysis. Then, w_0 can be given in the same form as Eq. (8), but with the coefficients a_{ij} replaced by b_{ij} . The latter are scaled to give the chosen $w_{0,max}$.

In design, maximum imperfection amplitudes $w_{0,\max}$ will normally be taken according to the values, $w_{0,\text{spec.}}$, specified in the relevant design codes, such as [1,2]. In order to compensate in part for the conservativeness implied by the displacement magnifier (Eq. (20)) for slender plates, a slenderness dependent $w_{0,\max}$ proposed by Brubak et al. [8] is adopted here. It is shown in Fig. 5 and defined by

$$\frac{w_{0,\max}}{w_{0,\text{spec.}}} = \begin{cases} \left(1 - \frac{1}{12}\bar{\lambda}^4\right) & \text{if } \bar{\lambda} \leq \sqrt{1.56} \\ 3/\bar{\lambda}^4 & \text{if } \bar{\lambda} \geq \sqrt{1.56} \end{cases} \quad (22)$$

where

$$\bar{\lambda} = \sqrt{\frac{\Lambda_Y}{\Lambda_{cr}^e}} \quad (23)$$

is the reduced slenderness. It is defined in terms of the load factor, Λ_Y , at which the von Mises' yield stress is reached ($\sigma_e^m = \Lambda_Y$), and the load factor, Λ_{cr}^e , of the first eigenvalue of the perfect plate.

6.3. Stress redistribution

Following the classical approach, large deflection theory (large rotations, but small in-plane strains) is used to capture the redistribution of stresses that takes place due to out-of-plane displacements. In this theory, the membrane strains in an imperfect plate can be written [16] as

$$\epsilon_x^m = u_{,x} + \frac{1}{2}w_{,x}^2 + w_{0,x}w_{,x} \quad (24)$$

$$\epsilon_y^m = v_{,y} + \frac{1}{2}w_{,y}^2 + w_{0,y}w_{,y} \quad (25)$$

$$\gamma_{xy}^m = u_{,y} + v_{,x} + w_{,x}w_{,y} + w_{0,x}w_{,y} + w_{0,y}w_{,x} \quad (26)$$

where w_0 is the initial imperfection, w is the additional displacements, u and v are the x - and y -displacements at the middle plane of the plate, respectively.

The strain compatibility equation for imperfect plates can now be obtained by the differentiation and combination of Eqs. (24)–(26). By substituting strains from Hooke's law for plane stresses into this equation, and introducing Airy's stress function $F(x, y)$, defined by $\sigma_x^m = F_{,yy}$, $\sigma_y^m = F_{,xx}$, $\tau_{xy}^m = -F_{,xy}$, the following nonlinear plate compatibility equation results:

$$\nabla^4 F = E(w_{,xy}^2 - w_{,xx}w_{,yy} + 2w_{0,xy}w_{,xy} - w_{0,xx}w_{,yy} - w_{0,yy}w_{,xx}). \quad (27)$$

This equation was given by Marguerre [16], and represents an extension of von Karman's plate theory. A solution of Eq. (27) of the form

$$F(x, y) = \Lambda \left(\frac{1}{2}\sigma_{x0}^m y^2 + \frac{1}{2}\sigma_{y0}^m x^2 - \tau_{xy0}^m xy \right) + \sum_{i=0}^{2M} \sum_{j=0}^{2N} f_{ij} \cos\left(\frac{i\pi}{L}x\right) \cos\left(\frac{j\pi}{b}y\right) \quad (28)$$

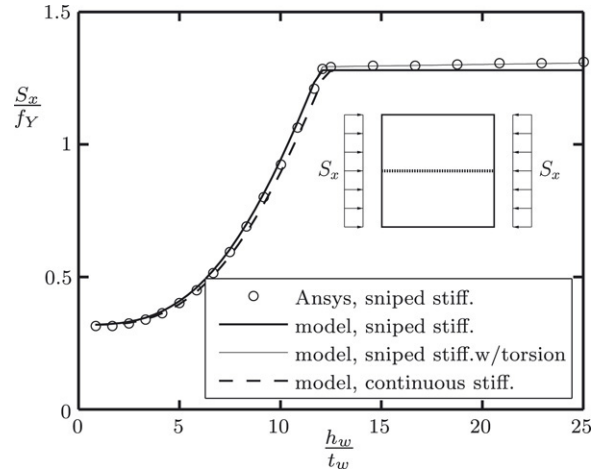


Fig. 6. Elastic buckling stress (ESL) in the global and local buckling range of a uniaxially loaded plate ($L = b = 2000$ mm, $t = 20$ mm) with an eccentric stiffener ($t_w = 12$ mm, height h_w , $b_e = 30t$).

was given by Levy [17] for perfect plates ($w_0 = 0$). Byklum et al. [4] showed that the same form can be used for imperfect plates and derived the stress amplitudes f_{ij} , given in Appendix A, for such plates. They are found by substituting $F(x, y)$, w and w_0 into Eq. (27).

Airy's stress function identically satisfies the in-plane equilibrium within each plate strip. To discuss the conditions at the interfaces, consider Eq. (28), where the first term is due to the external stresses. The second (summation) term represents the redistribution due to out-of-plane displacements (w_0 and w), and is a function of the load stage factor Λ through the amplitudes a_{ij} and b_{ij} . The second term varies smoothly across an interface between two strips (of different thickness), while the first term exhibits stress jumps at the interfaces. A consequence of this is that equilibrium will be satisfied only on average between two strips (of full length), and not along limited strip lengths.

Local inaccuracies in stresses near interfaces increase with the increasing dominance of the summation term in Eq. (28), i.e., with increasing plate slenderness since the displacements (w) increase with increasing slenderness. For very slender plates, possible effects on strength predictions are of minor concern, as the present model is rather conservative for such plates due to its neglect of the post-critical reserve strength.

7. Sniped vs. end-loaded stiffeners

Fig. 6 shows the buckling stresses (ESL) for a uniaxially loaded (S_x), simply supported, quadratic plate having constant thickness and one regular, eccentric flat bar stiffener (t_w , h_w) in the middle (parallel to S_x). The stiffener is either sniped or end-loaded (but with no rotational restraints at the ends). In the latter case, S_x is also applied to the stiffener area. The elastic material properties and modelling details are the same as given below (Section 9). With increasing stiffener stiffness, the buckling stress increases as the buckling mode changes from a fully global mode, through a mixed mode, to an almost fully local mode at the "threshold value", at which the rather flat plateau begins (at about $h_w/t_w = 12$ –13).

The moment of inertia I_e (Eq. (17)) is calculated with an effective width $b_e = 30t$. In the local buckling range, the model results would have increased slightly if the I_e -values had been calculated about the middle plane of the plate instead.

The effect on the results of end-loading on a continuous stiffener is also seen to be rather small in the considered case. This is particularly so for local plate buckling cases, to the right of the threshold value, where results for the sniped and the end-loaded stiffener (dashed line) coincide almost exactly. This was to be expected, since the stiffener–plate interface will remain nearly straight when local buckling occurs. The external loads on a stiffener will then only contribute negligibly to the potential energy, T . As a consequence, it makes little difference for the resulting buckling stresses acting on the plate whether the stiffeners are end-loaded or not in local plate buckling cases.

In global buckling cases, the difference is seen to be somewhat greater, but not significantly so. In this case, the smaller global buckling stress in the end-loaded stiffener case is almost completely compensated for by the greater load area. The resultant edge loadings, $P_{\text{cont.}} = S_{x,\text{cont.}}(bt + t_w h_w)$ and $P_{\text{sniped}} = S_{x,\text{sniped}}bt$ are found to be almost the same. For local plate buckling cases, the target in most practical design situations, the difference in total loading is simply equal to the additional load carried by the stiffener in the end loaded case.

8. Effect of torsional stiffness

The effect of including the torsional stiffness ($J = h_w t_w^3/3$) of the stiffener can be seen in Fig. 6 by comparing the results obtained by the present model for the sniped stiffener case with and without torsion included (full, thin line versus full, thick line). For global buckling modes, there is no effect since the stiffener does not rotate, due to symmetry. For local plate buckling, there are some, but very small beneficial effects. Local plate buckling results in the present model with torsional effects included, are almost identical to corresponding ANSYS results, which are also shown in the figure (open dots). Such torsional effects are conservatively neglected in the remainder of the paper.

9. Validation

The applicability of the presented model, incorporated into a Fortran computer program, has been assessed for many plate and stiffener dimensions. Elastic buckling stress limits (ESL) are verified against ESL results obtained by the finite element analysis computer program ANSYS [18] using Shell93 elements. Buckling strength limits (BSL) are compared with ultimate strength limits, here labelled USL, obtained from fully nonlinear ANSYS analyses (considering both geometric and material nonlinearity).

Ultimate strength limits (USL) are the maximum loads plates can carry without becoming unstable. For thin (slender) plates, they will give information about the reserve strength, beyond the BSL results. The BSL and the USL results should ideally converge as the plate thickness increases.

The specified imperfection is taken as $w_{0,\text{spec.}} = 5$ mm for the purpose of making comparisons. In the fully nonlinear

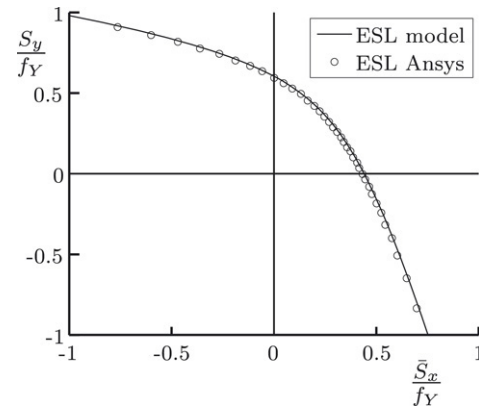


Fig. 7. ESL interaction curves for a stepped plate consisting of two plate strips of unequal width and thickness ($L/b_1/t_1 = 1000/1000/20$ mm, and $L/b_2/t_2 = 1000/500/10$ mm).

USL analyses, this value is used directly as the maximum imperfection amplitude ($w_{0,\text{max}} = w_{0,\text{spec.}} = 5$ mm). In the BSL calculations, on the other hand, the fictitious, slenderness dependent value $w_{0,\text{max}}$ according to Eq. (22) is used. The corresponding imperfection shapes are taken equal to the first eigenmode of the plate, as computed with ANSYS and the present model, respectively.

The elastic material properties used are $E = 208\,000$ MPa and $\nu = 0.3$, and the yield strength is $f_Y = 235$ MPa. In the fully nonlinear ANSYS analyses, a bilinear stress–strain relationship is used that is defined by the properties above, and additionally by a hardening modulus $E_T = 1000$ MPa. In the subsequent comparisons, the moment of inertia of the stiffeners is approximated by I_e about the middle plane (i.e., Eq. (17) with $z_c = 0$) and the torsional stiffness is neglected.

The displacement field in the present model is defined with 15 terms in each direction (i.e. 225 degrees of freedom). This generally provides sufficient numerical accuracy. The resulting strength predictions may be up to about 2% greater than those that would have been obtained with two to three times the number of terms in each direction. In many cases, the number of terms could be significantly reduced without reducing the accuracy noticeably. In comparison, in a typical USL analysis by ANSYS, the number of degrees of freedom used was about 20 000. Probably, sufficient accuracy could have been obtained with fewer degrees of freedom.

Selected results of the comparisons are presented in subsequent sections. They are limited to simply supported plates with eccentric or symmetric sniped stiffeners (free and not loaded at the ends). To provide severe test cases for the stepped plates, the relative difference in thickness between the thickest and thinnest strip in some of the plates is chosen to be rather large. Further, both regular and rather strongly irregular stiffener orientations are considered. Additional comparisons with ANSYS results are given by Brubak [15], where clamped plates are also considered.

10. ESL predictions

Typical elastic buckling stresses (eigenvalues) are shown by the interaction curves in Fig. 7, obtained for an unstiffened

Table 1
Dimensions (mm) of plates with stepwise constant plate thickness and two inclined, eccentric stiffeners

	L	b	t_1	t_2	t_3	h_w	t_w	b_f	t_f
Plate 1	1000	2400	25	20	15	200	15	150	25
Plate 2	1200	2400	25	20	15	200	15	150	25
Plate 3	1000	3000	20	18	16	200	16	100	16

Table 2
Dimensions (mm) of plates with stepwise constant plate thickness and two symmetric stiffeners with regular orientation

	L	b	t_1	t_2	t_3	h_w	t_w	b_f	t_f
Plate 4	3000	3300	30	28	26	300	10	150	20
Plate 5	3000	2100	24	22	20	300	10	150	20
Plate 6	3000	2100	16	14	12	300	8	100	10

plate consisting of two very different plate strips. The present ESL model does not neglect any energy contributions in the case of unstiffened plates. The results will therefore converge towards the exact solution as the number of degrees of freedom increases. The excellent agreement with the ANSYS results shows that the assumed displacement field, defined over the entire plate, is clearly acceptable with the present choice of degrees of freedom.

For stiffened plates, the agreement cannot be expected to be equally good, due to the neglect of some energy contributions and approximations in initial, reference stress computations (neglect of axial stiffener stiffness). However, as will be seen in the ESL results shown below for several stepped plates (Tables 1 and 2), the agreement is still considered to be very good for biaxial stress combinations of interest (Figs. 9 and 10).

11. BSL predictions — Inclined eccentric stiffeners

A number of plates with three strips and two inclined, eccentric, sniped T-section stiffeners (Fig. 2(b)) have been analysed. Selected results for the plates defined in Table 1 and Fig. 9(a) will be presented and discussed. The stiffener cross-sections satisfy the slenderness requirements in Eq. (1) in order to avoid premature local stiffener buckling.

The first buckling mode calculated by the present model and by the finite element model has been found to be quite similar in each case considered. A typical case is shown in Fig. 8(a) and (b). The displacements are largest in the thinnest plate strip. The mode shown can be considered as a local plate buckling mode, as the out-of-plane plate displacements along the stiffeners are small. This is a consequence of the chosen stiffeners, which apparently are sufficiently stiff to prevent a global buckling mode. The same is found to be the case for the other plates in Table 1. The main difference between the models is that the finite element model accounts for the sideways deflections of the stiffeners and of their torsional and axial stiffnesses.

In Fig. 9, biaxial load interaction curves are given for buckling strengths (BSL), elastic buckling stresses (ESL) (which have been discussed above), and the “yield limit” according to the von Mises yield criterion for the material as such. The latter represents a maximum strength limit.

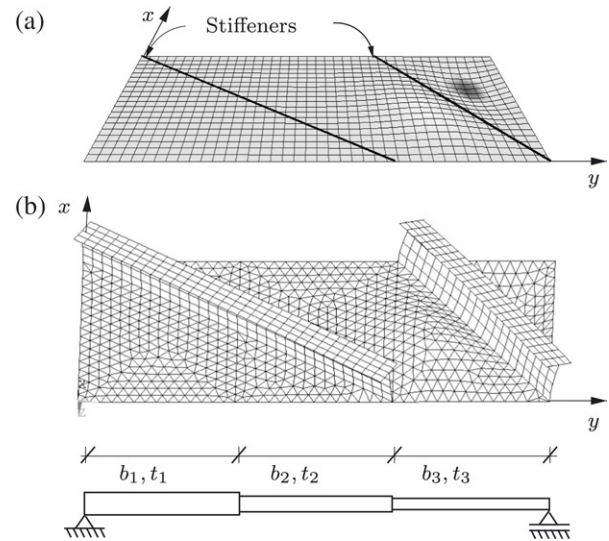


Fig. 8. First buckling mode of plate 1 subjected to a uniaxial external stress S_y , calculated by (a) the present model and (b) Ansys.

In the context of the buckling strength, the most relevant loading situations are those with uniaxial or biaxial compressive stresses (in the first quadrant).

Also shown in the figure are ultimate strength (USL) results. These are seen to be close to the BSL results for the considered plates, which have relatively small to intermediate slenderness values. The slenderness $\bar{\lambda}$ varies along the interaction curves, but it is smaller than 1.05 for all load combinations. The corresponding relative imperfection amplitude $w_{0,\max}/w_{0,\text{spec}}$ varies between 0.90 and 1. Thus, the reduction of the imperfection amplitude in the BSL procedure is small in these cases. More slender plates, for which BSL results will become more conservative relative to USL results, are discussed below.

12. BSL predictions — Regular, symmetric stiffeners

For uni-directionally stepped plates, it is believed that regular stiffeners represent a more common stiffener arrangement than inclined stiffeners. Similar results to those presented above have been obtained for a number of such plates, for which preliminary results were given in [19]. Selected results, for the plates with three strips and two regular, symmetric stiffeners defined in Table 2 and Fig. 10(a), are shown in Fig. 10(b), (c) and (d). In order to avoid local stiffener buckling, the stiffener cross-section requirements in Eq. (1) are satisfied. Also, for the plates considered here, closer examinations show that the first buckling modes are local plate buckling modes.

The BSL and USL results are close to each other for plates 4 and 5, which have relatively small to intermediate reduced slenderness values. For instance, for plate 5, the maximum reduced slenderness is approximately $\bar{\lambda} = 1.17$ (for $\bar{S}_x = 1.67S_y$). The corresponding imperfection amplitude is $w_{0,\max} = 0.84w_{0,\text{spec}}$ according to Eq. (22).

For plate 6, the maximum reduced slenderness is approximately 2.36 (for $\bar{S}_x = 1.43S_y$), which is representative of a very slender case. The corresponding imperfection amplitude is $w_{0,\max} = 0.10w_{0,\text{spec}}$, which is, physically

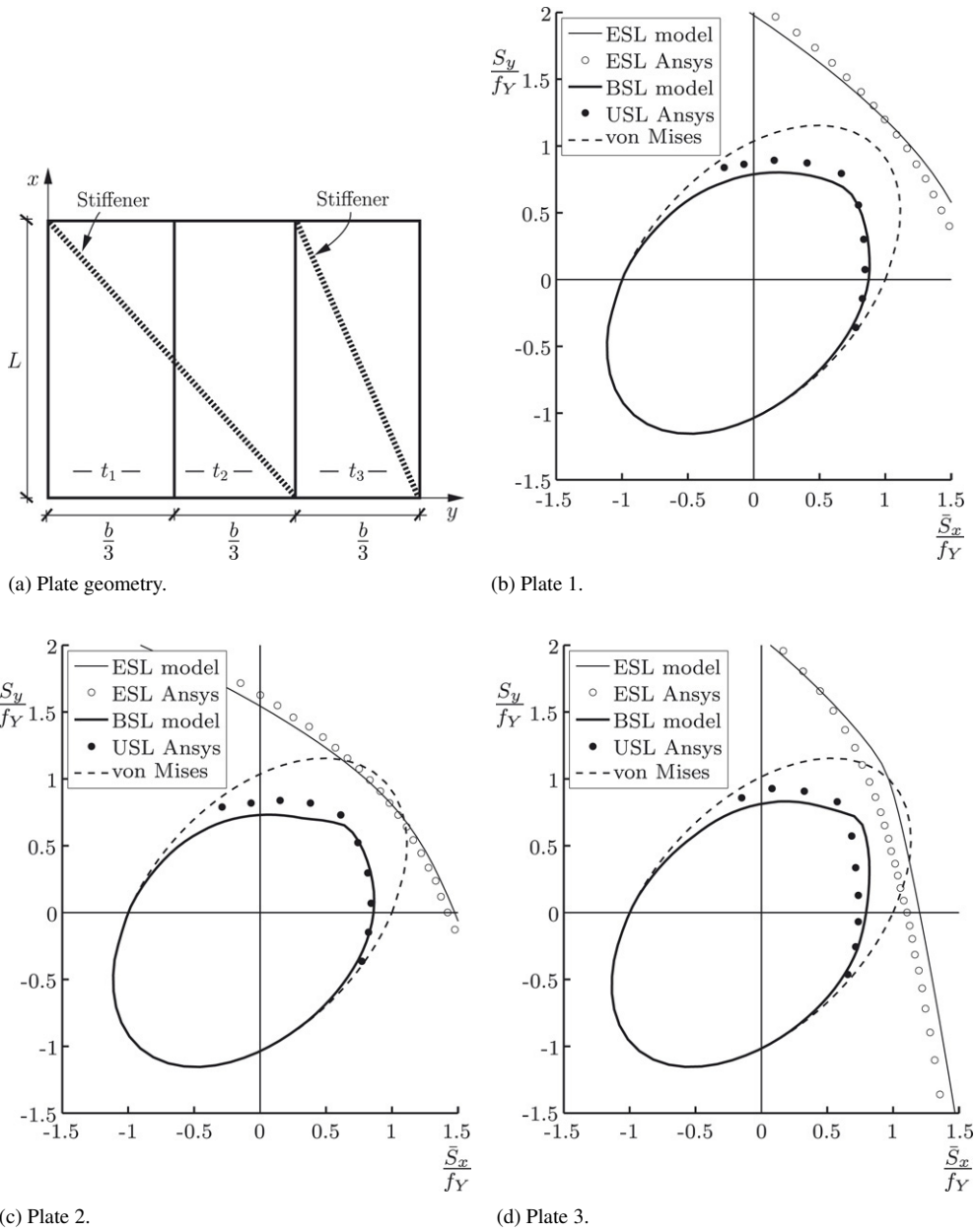


Fig. 9. Interaction curves in the stress space S_x – S_y for plates no. 1, 2 and 3, with stepwise constant thickness and with two eccentric, inclined stiffeners.

speaking, unreasonably small. Even so, the BSL results calculated by the present method are still conservative compared to the fully nonlinear USL results. The latter is in this case twice as large as the BSL results.

The reason for the conservativeness in the BSL results for slender plates is (as mentioned before) that the present BSL model is not able to capture the post-critical (reserve) strength. Therefore, the present BSL model is most feasible in practical design cases in which loading in the post-buckling range is not accepted.

13. Improved initial shear stress formulation

For plates with larger thickness variations, a more refined analysis than that presented previously (Section 4) must be performed in order to find initial internal stresses due to external

shear loading. An elastic static analysis can be performed using the Rayleigh–Ritz method with assumed in-plane displacement fields. For instance, the displacements u and v in the x - and y -direction, respectively, can be taken as

$$u(x, y) = u_0 \frac{y}{b} + \sum_{i=1}^{M_u} \sum_{j=1}^{N_u} u_{ij} \sin\left(\frac{\pi i x}{L}\right) \sin\left(\frac{\pi j y}{b}\right) \quad (29)$$

$$v(x, y) = \sum_{i=1}^{M_v} \sum_{j=1}^{N_v} v_{ij} \sin\left(\frac{\pi i x}{L}\right) \sin\left(\frac{\pi j y}{b}\right) \quad (30)$$

where u_0 , u_{ij} and v_{ij} are displacement amplitudes. When the unknown displacement amplitudes are found, the strains can be computed and, finally, the internal stresses in the plate can be computed using Hooke’s law. These stresses must be added

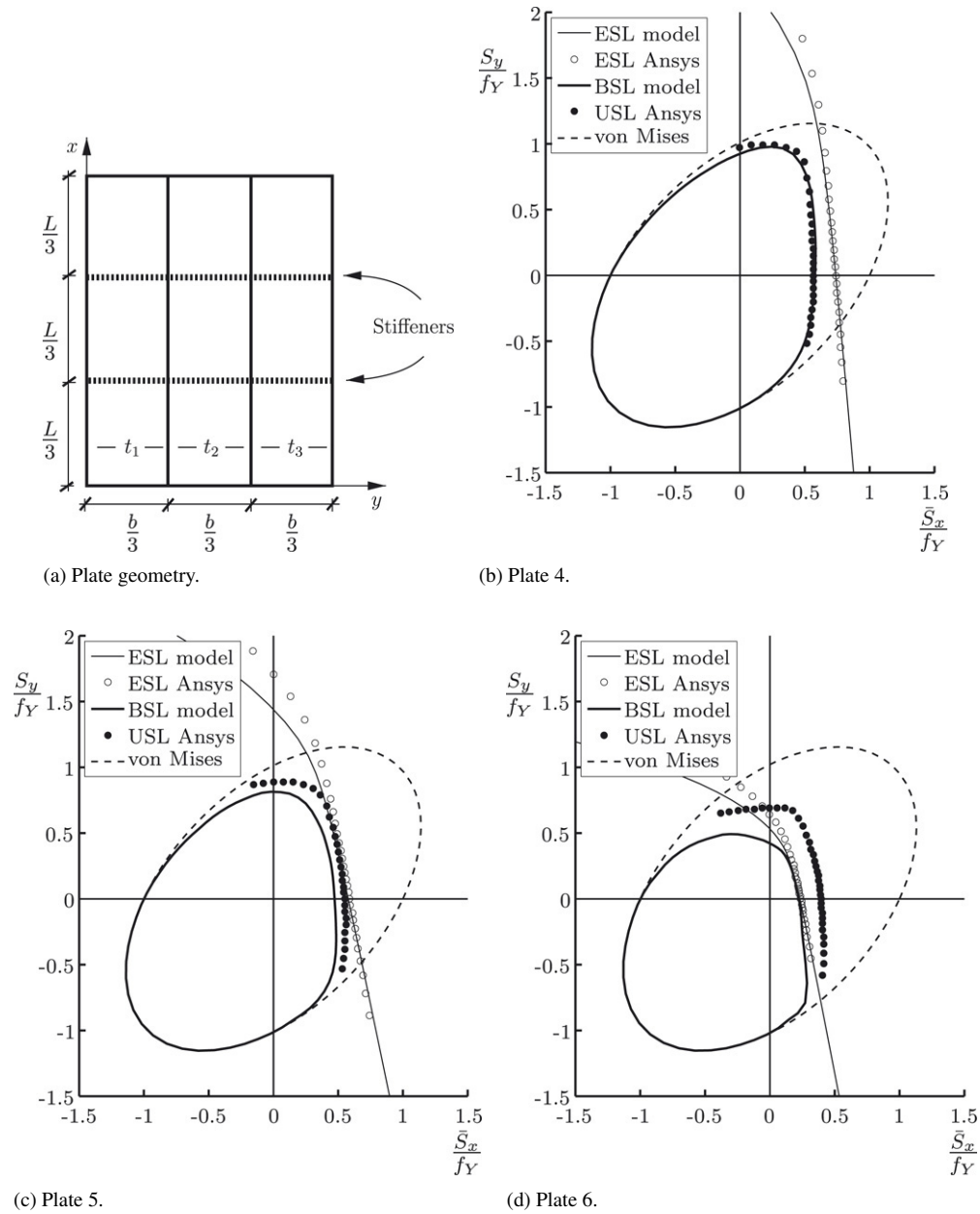


Fig. 10. Interaction curves in the stress space S_x-S_y for plates no. 4, 5 and 6, with stepwise constant thickness and with two symmetric, regular stiffeners.

to the in-plane axial stresses due to biaxial loading found by the procedure in Section 4. With this approach, portions of the present energy expressions will need to be revised, and will become more complicated than they presently are.

14. Lateral pressure

The presented model can be extended to strength computations for plates that also are subjected to a lateral loading $p = p(x, y)$ of a given value, i.e., it is not increased proportionally with the in-plane external loads. In addition to the computational steps presented previously, this requires a separate Rayleigh–Ritz analysis based on an assumed displacement field in order to calculate: (1) the out-of-plane displacement w_p , and (2) the corresponding internal stresses (“ σ_p ”) due to the lateral pressure acting alone. In this

calculation, the potential strain energy of a plate strip is equal to Eq. (11) with w replaced by w_p , and the potential energy due to a lateral pressure p alone is

$$T_p = - \int_0^b \int_0^L p w_p \, dy \, dx. \tag{31}$$

The lateral pressure does not affect the eigenvalues. In the BSL procedure, the calculated displacement w_p must be added to the imperfection w_0 such that $w_0 + w_p$ can be considered a total initial imperfection. Further, the calculated internal stresses (“ σ_p ”) due to the lateral pressure alone must be added to the internal stresses due to the external in-plane stresses. With lateral pressure included, the present strength criterion may have to be revised. For example, it may be necessary to include bending stresses in the criterion.

15. Concluding remarks

An approximate method for global and local buckling strength (BSL) analysis of stepped plates with arbitrary stiffener orientations has been presented. Out-of-plane displacements have been estimated using an approximate displacement magnifier, and plate failure has been estimated using von Mises' yield criterion. The assumed displacement field implies that equilibrium is satisfied between the plate strips only on average. For the implementation of a suggested, more advanced shear loading representation, further work is required. Also, extension to include lateral loading remains to be done.

The applicability and versatility of the presented model are documented for various plate geometries, and computed BSL results are validated against fully nonlinear USL analyses. The BSL predictions are generally conservative, particularly for slender plates. This is due to the use of the approximate displacement magnifier, which results in buckling strengths that never exceed the elastic buckling loads. Consequently, the postbuckling (reserve) strengths for slender plates are not accounted for. Although conservative, this may be a sound theoretical treatment in design situations in which it is not accepted that the structural elements buckle elastically.

The method is computationally very efficient. Using a computer code that has not yet been optimised, the computer time for a BSL prediction for a given loading is typically 1–2 s on a medium fast computer (1.5 GHz processor, 512 MB RAM). Compared to nonlinear ultimate strength (USL) results obtained using ANSYS, the presented method is typically more than 1000 times faster for the same problem. Speed is always an advantage, particularly in optimisation and reliability studies, and in other situations requiring larger numbers of case studies. The size of the computer program needed for the method is limited, and the amount of input data required is minimal. Due to such factors, the method is suitable for incorporation into computerised analysis and design codes. A constant thickness version is already included in a code labelled PULS [9], and can be downloaded from <http://www.dnv.com>.

Acknowledgements

The authors would like to thank dr.scient. Eivind Steen and dr.ing. Eirik Byklum, both at DNV, for initially suggesting the topic of the paper, for their interest and discussions, and additionally for making a computer subroutine for stress calculations available for use in this study. Discussions with dr.ing. Geir Skeie, especially on shear, is also greatly appreciated.

Appendix A

A.1. Coefficients in Airy's stress function

The coefficients f_{ij} in Airy's stress function are defined by

$$f_{ij} = \frac{E}{4(i^2 \frac{b}{L} + j^2 \frac{L}{b})^2} \sum_{r=1}^M \sum_{s=1}^N \sum_{p=1}^M \sum_{q=1}^N c_{rspq} (a_{rs} a_{pq} + a_{rs} b_{pq} + a_{pq} b_{rs}) \quad (\text{A.1})$$

where f_{00} is zero, a_{rs} and b_{pq} are the amplitudes of w and w_0 , respectively, and c_{rspq} are integers as given below.

$$\text{If } \pm(r-p) = i \text{ and } s+q = j, \text{ or } r+p = i \text{ and } \pm(s-q) = j \\ c_{rspq} = rspq + r^2 q^2. \quad (\text{A.2})$$

$$\text{If } r+p = i \text{ and } s+q = j, \text{ or } \pm(r-p) = i \text{ and } \pm(s-q) = j \\ c_{rspq} = rspq - r^2 q^2. \quad (\text{A.3})$$

For other cases

$$c_{rspq} = 0. \quad (\text{A.4})$$

More details of the derivation of the coefficients f_{ij} can be found in the literature [4].

A.2. Definition of $H_1(j, l)$, $H_2(j, l)$ and $H_3(j, l)$

$$H_1(j, l) = \int_{y_{s1}}^{y_{s2}} \sin\left(\frac{\pi j}{b} y\right) \sin\left(\frac{\pi l}{b} y\right) dy \quad (\text{A.5})$$

$$H_2(j, l) = \int_{y_{s1}}^{y_{s2}} \cos\left(\frac{\pi j}{b} y\right) \cos\left(\frac{\pi l}{b} y\right) dy \quad (\text{A.6})$$

$$H_3(j, l) = \int_{y_{s1}}^{y_{s2}} \cos\left(\frac{\pi j}{b} y\right) \sin\left(\frac{\pi l}{b} y\right) dy \quad (\text{A.7})$$

$$H_4(i, k) = \int_0^L \cos\left(\frac{\pi i}{L} x\right) \sin\left(\frac{\pi k}{L} x\right) dy. \quad (\text{A.8})$$

The results of these integrals are given below.

$$\text{If } j \neq l \\ H_1(j, l) = \frac{b}{2\pi(j^2 - l^2)} \\ \times \left((j+l) \sin\left(\frac{\pi(j-l)}{b} y\right) - (j-l) \sin\left(\frac{\pi(j+l)}{b} y\right) \right) \Big|_{y_{s1}}^{y_{s2}}. \quad (\text{A.9})$$

If $j = l$

$$H_1(j, j) = \left(\frac{y}{2} - \frac{b}{2\pi j} \cos\left(\frac{\pi j}{b} y\right) \sin\left(\frac{\pi j}{b} y\right) \right) \Big|_{y_{s1}}^{y_{s2}}. \quad (\text{A.10})$$

If $j \neq l$

$$H_2(j, l) = \frac{b}{2\pi(j^2 - l^2)} \\ \times \left((j+l) \sin\left(\frac{\pi(j-l)}{b} y\right) + (j-l) \sin\left(\frac{\pi(j+l)}{b} y\right) \right) \Big|_{y_{s1}}^{y_{s2}}. \quad (\text{A.11})$$

If $j = l$

$$H_2(j, j) = \left(\frac{b}{2\pi j} \cos\left(\frac{\pi j}{b} y\right) \sin\left(\frac{\pi j}{b} y\right) + \frac{y}{2} \right) \Big|_{y_{s1}}^{y_{s2}}. \quad (\text{A.12})$$

If $j \neq l$

$$H_3(j, l) = -\frac{b}{2\pi(j^2 - l^2)} \\ \times \left((j+l) \cos\left(\frac{\pi(j-l)}{b} y\right) + (j-l) \cos\left(\frac{\pi(j+l)}{b} y\right) \right) \Big|_{y_{s1}}^{y_{s2}}. \quad (\text{A.13})$$

If $j = l$

$$H_3(j, j) = \left(\frac{b}{2\pi j} \sin^2 \left(\frac{\pi j}{b} y \right) \right) \Big|_{y=1}^{y=2}. \quad (\text{A.14})$$

If $i \neq k$

$$H_4(i, k) = -\frac{L}{2\pi} \times \left(\frac{\cos((k+i)\pi) - 1}{k+i} + \frac{\cos((k-i)\pi) - 1}{k-i} \right). \quad (\text{A.15})$$

If $i = k$

$$H_4(i, i) = 0. \quad (\text{A.16})$$

References

- [1] prEN 1993-1-5. Eurocode 3: Design of steel structures. Part 1.5: Plated structural elements. Brussels: CEN, European Committee for Standardisation; 2005.
- [2] Det Norske Veritas. DNV Rules for classification of ships. Høvik (Norway): Det Norske Veritas; 2002.
- [3] Det Norske Veritas. Recommended practice DNV-RP-C201. Buckling strength of plated structures. Høvik (Norway); 2002.
- [4] Byklum E, Amdahl J. A simplified method for elastic large deflection analysis of plates and stiffened panels due to local buckling. *Thin-Walled Structures* 2000;40(11):925–53.
- [5] Byklum E, Steen E, Amdahl J. A semi-analytical model for global buckling and postbuckling analysis of stiffened panels. *Thin-Walled Structures* 2004;42(5):701–17.
- [6] Steen E. Application of the perturbation method to plate buckling problems. Research report in mechanics, No. 98-1. Norway: Mechanics Division, Dept. of Mathematics, University of Oslo; 1998. 60 pp.
- [7] Steen E. Buckling of stiffened plates using a Shanley model approach. Research report in mechanics, No. 99-1. Norway: Mechanics Division, Dept. of Mathematics, University of Oslo; 1998. 84 pp.
- [8] Brubak L, Helleland J, Steen E. Semi-analytical buckling strength analysis of plates with arbitrary stiffener arrangements. *Journal of Constructional Steel Research* 2007;63(4):532–43.
- [9] Steen E, Byklum E, Vilming KG, Østfold TK. Computerized buckling models for ultimate strength assessments of stiffened ship hull panels. In: Proceedings of the ninth international symposium on practical design of ships and other floating structures. 2004. p. 235–42.
- [10] Paik JK, Lee MS. A Semi-analytical method for the elastic-plastic large deflection analysis of stiffened panels under combined biaxial compression/tension, biaxial in-plate bending, edge shear, and lateral pressure loads. *Thin-Walled Structures* 2005;43(3):375–410.
- [11] Azhari M, Shahidi AR, Saadatpour MM. Local and post local buckling of stepped and perforated thin plates. *Applied Mathematical Modelling* 2005;29(7):633–52.
- [12] Xiang Y, Wei GW. Exact solutions for buckling and vibration of stepped rectangular Mindlin plates. *International Journal of Solids and Structures* 2004;41(1):279–94.
- [13] prEN 1993-1-1. Eurocode 3: Design of steel structures. Part 1.1: General rules and rules for buildings. Brussels: CEN, European Committee for Standardisation; 2003.
- [14] Timoshenko SP, Gere JM. Theory of elastic stability. 2nd ed. McGraw-Hill Book Company; 1963.
- [15] Brubak L. Semi-analytical buckling strength analysis of plates with constant or varying thickness and arbitrarily oriented stiffeners. Research report in mechanics, No. 05-6. Norway: Mechanics Division, Dept. of Mathematics, University of Oslo; 2005. 65 pp.
- [16] Marguerre K. Zur theorie der gekrümmten platte grosser formänderung. In: Proceedings of the 5th international congress for applied mechanics. 1938. p. 93–101.
- [17] Levy S. Bending of rectangular plates with large deflections. Report 737. NACA. 1942.
- [18] ANSYS Inc. ANSYS documentation 9.0. Southpointe, Canonsburg, PA; 2004.
- [19] Brubak L, Helleland J. Computational buckling strength analysis of stiffened plates with varying thickness. In: Bergan P, García J, Onâte E, Kvamsdahl T, editors. Proceedings of the international conference on computational methods in marine engineering. 2005. p. 355–64.